Single Quality Factor for Enthalpy-Entropy Compensation, Isoequilibrium and Isokinetic Relationships

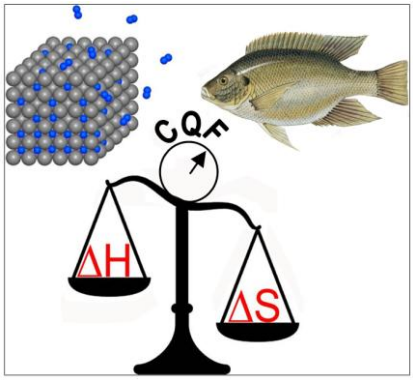

Entropy-Enthalpy Compensation : We introduce the Compensation Quality Factor CQF to determine whether experimental data imply a physical relation between the enthalpy and entropy of a series of similar reactions. CQF describes both the degree of coalescence at the isoequilibrium temperature and the nature of the Entropy-Enthalpy Compensation (statistical or non-statistical). The same approach is used to establish the existence of a genuine isokinetic relationship, both in the hydrogenation of metals and enzyme catalysis in fish muscles.

Single Quality Factor for Enthalpy-Entropy Compensation, Isoequilibrium and Isokinetic Relationships

Ronald Griessen[a],*, Christiaan Boelsma[b], Herman Schreuders[c], Chase P. Broedersz[d], Robin Gremaud[e] and Bernard Dam[c],*

§

Abstract

Enthalpy-entropy compensation (*EEC*) is very often encountered in chemistry, biology and physics. Its origin is widely discussed since it would allow e.g. a very accurate tuning of the thermodynamic properties as a function of the reactants. However, *EEC* is often discarded as a statistical artefact, especially when only a limited temperature range is considered. We show that the likeliness of a statistical origin of an *EEC* can be established with a Compensation Quality Factor (*CQF*) that depends only on the measured enthalpies and entropies and the experimental temperature range. This is directly derived from a comparison of the *CQF* with threshold values obtained from a large number of simulations with randomly generated Van 't Hoff plots. The value of *CQF* is furthermore a direct measure of the existence of a genuine isoequilibrium or isokinetic relationship.

[a] Prof.Dr. R. Griessen, Condensed Matter Physics, Faculty of Sciences, VU University Amsterdam, De Boelelaan 1081, 1081 HV Amsterdam, The Netherlands
[b] Dr. Christiaan Boelsma, Tata Steel, Research and Development, PO Box 10000, 1970 CA IJmuiden, The Netherlands
[c] Ing. Herman Schreuders, Prof. Dr. Bernard Dam, Materials for Energy Conversion and Storage, Department of Chemical Engineering, Faculty of Applied Sciences, Delft University of Technology, Van der Maasweg 9, 2629 HZ Delft, The Netherlands
[d] Prof.Dr. Chase P. Broedersz, Arnold-Sommerfeld-Center for Theoretical Physics and Center for NanoScience, Ludwig-Maximilians-Universität München, 80333 Munich, Germany
[e] Dr. Robin Gremaud, ABB Switzerland Ltd, Corporate Research, Segelhofstrasse 1K, 5405 Baden-Dättwil, Switzerland

*corresponding authors. E-mail: b.dam@tudelft.nl and r.p.griessen@vu.nl

1 Introduction

There is a longstanding debate in the literature regarding the physical basis of the so-called enthalpy-entropy compensation (*EEC*), which is observed in a wide range of fields in chemistry[1, 2, 3, 4, 5, 6,7,8] , biology[9, 10, 11, 12, 13, 14, 15] and solid-state physics[16, 17, 18, 19] . *EEC* describes a linear relation between two thermodynamic parameters, the enthalpy ΔH and entropy ΔS, of a series of similar reactions. Examples include the denaturation of closely related proteins, reactions in slightly varying solvents, or reactions of hydrogen with metal alloys[20]. While there is a wealth of data sets available, it is unclear which ΔH-ΔS correlations are strong enough to pursue a quest for the physical basis of the related enthalpy-entropy compensation.

Apart from its theoretical significance, in practice, the *EEC* effect would allow for the tuning of thermodynamic parameters, such as e.g. necessary for the design of an ideal sorption material for hydrogen storage. Such a material requires a hydrogen equilibrium pressure above 1 bar at around 300 K. *EEC* would help the discovery of materials combining this equilibrium pressure with an enthalpy of formation less negative than the -40 kJ/molH_2 of present storage systems. This would reduce the enormous heat load involved when fast charging a metal hydride based storage tank.

EEC is traditionally characterized by the slope of the ΔH-ΔS plot, the so-called compensation temperature $T_{comp} = \mathrm{d}(\Delta H)/\mathrm{d}(\Delta S)$, where all compositions of a particular set of reactions have e.g. the same equilibrium pressure. Interestingly, most observed compensation effects have a T_{comp} close to the harmonic mean of the experimental temperature, T_{hm}

$$T_{hm} = \left(\frac{1}{M} \sum_{j=1}^{M} \frac{1}{T_j} \right)^{-1} \qquad (1)$$

where T_j with j=1,...M, is the temperature of the *j-th* measurement. Hence, several authors have claimed that when $T_{comp} \approx T_{hm}$, statistical and/or experimental errors are causing these compensation effects[21, 22, 23, 24, 25, 26, 27, 28, 29, 30]. Indeed, whenever data are collected in a small region of the pressure-temperature plane[26] the measured Van 't Hoff plots of a series of reactions have the tendency to cross within the experimental region and the corresponding ΔH versus ΔS plot is approximately a straight line suggesting *EEC* behaviour (see Section 3 in Suppl. Inf.).

In a more quantitative approach, Krug et al.[31, 32] derived a statistical test to compare the harmonic mean experimental temperature T_{hm} with the interval $[T_{comp}-t\sigma, T_{comp}+t\sigma]$. Here, σ is the standard error in T_{comp} and the Student's *t-value* depends on the chosen confidence level and the number of samples, i.e. the number of (ΔH,ΔS) data pairs. For a 95% confidence level t is close to 2 for large data sets. If T_{hm} falls within this temperature interval Krug et al. consider that the *EEC* is probably of statistical nature at a 95% confidence level. However, this approach does not predict the degree of coalescence of Van 't Hoff lines observed near T_{comp}. It therefore does not provide information about the isoequilibrium relationship.

For a hypothetical, perfect *EEC* all related Van 't Hoff plots (i.e. plots of the logarithm of the pressure versus the inverse absolute temperature from which ΔH and ΔS are determined for each composition) should have a common intersection point at T_{comp}. Clearly, such a unique common intersection point is never realized in practice as a result of ever-present experimental errors.

Hence, one would expect a simple correlation between the presence of a trustworthy compensation temperature and a coalescence of the Van 't Hoff lines. However, Liu and Guo conclude in their much cited review article[4] that the Enthalpy-Entropy compensation effect and the isoequilibrium effect are not necessarily synonymous (see for a more detailed discussion Section 1 in Suppl. Inf.).

At variance with this claim we show in the present article that both the nature of the *EEC* (statistical or non-statistical) *and* the degree of coalescence of Van 't Hoff lines can be quantitatively characterized by a *single* parameter calculated from the ΔH and ΔS values derived from the measured ln*P* versus *1/*T lines of a set of *N* samples. We analytically calculate the variance in ln*P* for the set of the *N* investigated samples and determine the temperature T_{min} at which the variance of ln*P* reaches a minimum. The variance of ln*P* at $T = T_{min}$ is a direct measure of the degree of coalescence of the Van 't Hoff plots. The ratio of the variance of ln*P* at $T = T_{min}$ normalized to the largest experimentally measured ln*P* variance defines a Compensation Quality Factor *CQF* that characterizes quantitatively the extent of the crossing region of Van 't Hoff lines. The *CQF* is by definition unity for perfect compensation (T_{min} equal to T_{comp}) and tends towards zero when Van 't Hoff lines do not come close to a single crossing.

Remarkably, it appears that the same *CQF* also reveals information on the question whether the observed *EEC* is statistical in nature or not. For the hypothetical case of statistically independent randomly generated Van 't Hoff lines we define a threshold *CQF* value γ which depends only on the number of samples *N* and the chosen confidence level. For a confidence level as high as 99% we find for example $\gamma = 0.67$ for a set of $N = 10$ samples. This means that 99% of all *CQF* random simulation values are below 0.67 or, equivalently, that there is only a 1% probability that the *EEC* of an experimental data set for $N = 10$ samples with $CQF > 0.67$ is of a statistical nature. In other words, there is a 99% probability that the observed *EEC* has a genuine (i.e. physical, chemical or biological) origin.

We demonstrate our new analytical framework using experimental pressure-composition data on the hydrogenation of two specific metal hydrides, Mg-Ti-H thin films and Pd-H nanocubes. The data set for 67 Mg-Ti alloy compositions is characterized by a $T_{comp} \cong 470$ K that falls *within* the experimental temperature range 348 < T < 473 K. The data for the Pd-H nanocubes recently published by Syrenova *et al*.[33] have a $T_{comp} \cong$ 283 K that falls clearly *outside* their experimental temperature range 303 < T < 333 K. Consequently one is tempted to conclude that a real ΔH-ΔS compensation exists only for the Pd nanocubes. However, it turns out that the contrary is borne out by our analysis: a genuine ΔH-ΔS compensation with a well-defined crossing of Van 't Hoff plots and a high value for $CQF \cong 0.94$ is found for the Mg-Ti alloys while a large spread of equilibrium pressures at T_{comp} and consequently a low value for $CQF \cong 0.26$ is found for the Pd-nanocubes.

In a second step we show that our method is also applicable to kinetic studies and the determination of the isokinetic temperature. The *CQF* is in this case a measure of the extent of the crossing region of Arrhenius plots, i.e. plots of the logarithm of the reaction rate versus the inverse temperature. The *CQF* is now entirely determined by the activation energy and pre-factor data determined from kinetic measurements (Arrhenius plots), and the temperature range of the experiments. We illustrate this case by analysing literature data on both hydrogen absorption

kinetics of magnesium-based samples[28] and the thermodynamic activation data of fish myofibrillar ATPase enzyme[34].

We stress that the key purpose of our work is to identify the likeliness of a non-statistical origin of the observed *EEC*, which would point to a fundamental thermodynamic relation. In addition, the *CQF* tells experimentalists whether it is worth to aim for isoequilibrium conditions or search for new compositions based on an extrapolated ΔS versus ΔH curve.

2 Results and Discussion

Although the concept of the *CQF* could be defined in a purely formal way we choose to introduce it step-by-step within the context of metal-hydrides. *EEC* is observed in various metal hydride systems.[20, 35, 36, 37, 38, 39, 40]. A typical metal hydride exists in two phases. At low hydrogen pressures, hydrogen forms a solid solution with the metal host (α-phase). Upon increasing the hydrogen pressure, the hydrogen concentration hardly increases until a certain pressure, the plateau pressure *P* at which the dilute α-phase coexists with the hydrogen-rich β-phase. The changes in enthalpy *ΔH* and entropy *ΔS* between the α- and the β-phases are obtained by fitting the temperature dependence of *P* to the Van 't Hoff relation:

$$\ln\left(\frac{P}{P_0}\right) = \frac{\Delta H}{RT} - \frac{\Delta S}{R} = h\left(\frac{1}{T}\right) - s \qquad (2)$$

here P_0 is the pressure at standard conditions, *R* the gas constant, and *ΔH* and *ΔS* are expressed per mole H_2. Note, that the determination of the entropy requires extrapolation over a large temperature range. In general hydrogen absorption in metals is measured in one sample at the time. The study of an *EEC* requires a relatively large number of samples which induces statistical errors related to the temperature and H_2 pressures of each experiment. In order to avoid this source of statistical errors we choose to measure a large number of samples *simultaneously* by means of Hydrogenography (see Section 4). The results obtained with this technique for the hydrogen absorption in 67 Mg-Ti thin films are given in Section 2.1. These results are contrasted with those of a recently published study on Pd-nanocubes in Section 2.2.

2.1 Enthalpy-entropy compensation in Mg-Ti hydrides.

To simultaneously investigate a large range of thin film alloy compositions, we measure the hydrogen absorption process by means of Hydrogenography[20]. In this optical method we obtain the logarithm of the applied hydrogen pressure as a function of the hydrogen concentration for hundreds of compositions in a single experiment. In these compositional gradient thin films samples, the change in optical transmission $\mathcal{T}$ is a measure of the hydrogen concentration. We thus obtain **P**ressure-optical **T**ransmission-**I**sotherms PTIs, similar to the more commonly obtained **P**ressure-**C**omposition-**I**sotherms PCIs[41].

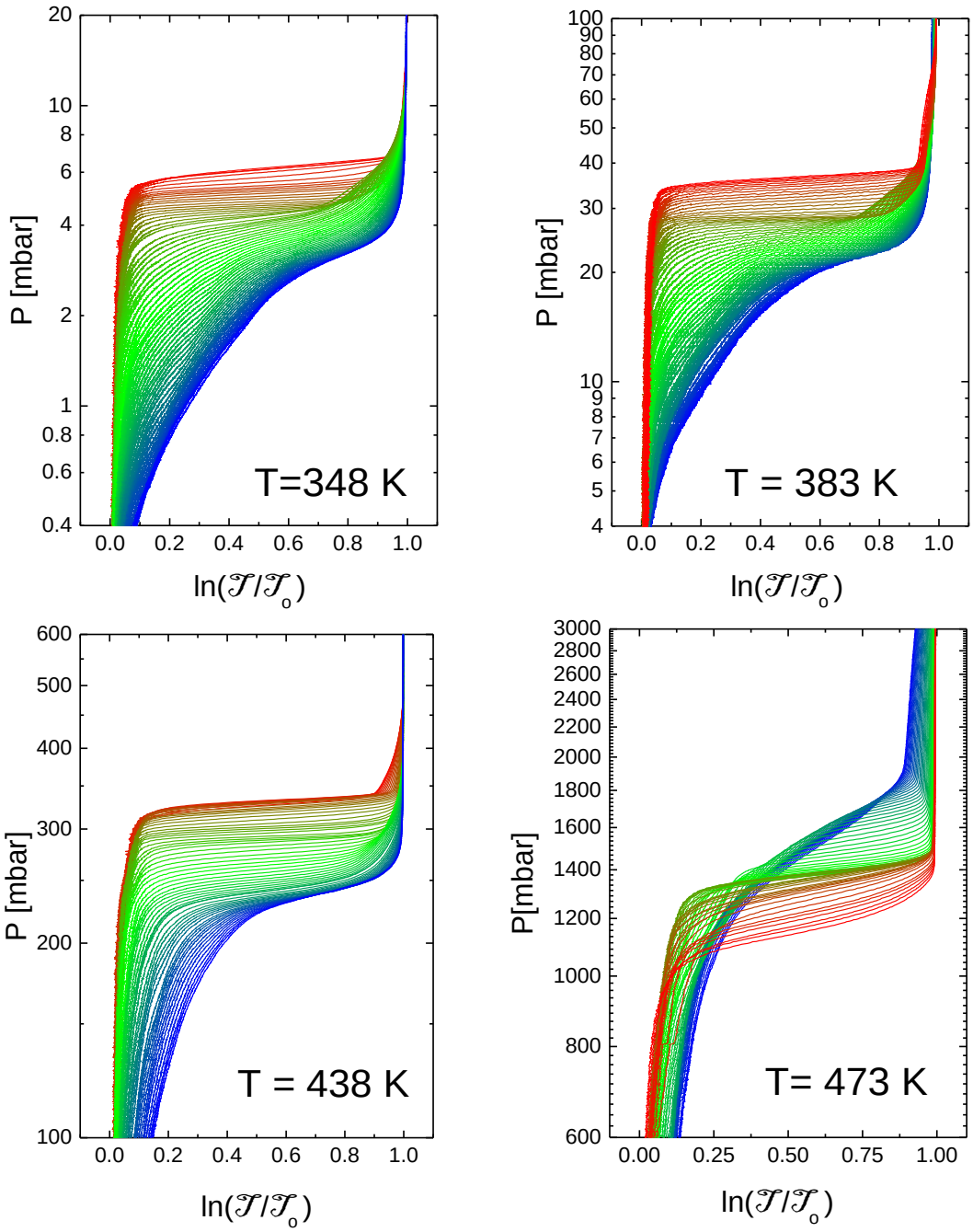

Figure 1: Pressure-optical Transmission-Isotherms PTIs for 67 Mg_yTi_{1-y} alloys with 0.62 < y < 0.81 (1st hydrogenation) at 348, 383, 438 and 473 K measured simultaneously by means of Hydrogenography. The colours correspond to the Mg concentration increasing in steps of Δy = 0.00288 from 0.62 (blue) to 0.81 (red). The preparation of the Mg_yTi_{1-y} (0.62 ≤ y ≤ 0.81) thin film gradient samples is described in the Experimental Section 4. The logarithm of the optical transmission change ln(𝒯/𝒯₀) is linearly related to the hydrogen concentration in the Mg_yTi_{1-y} gradient films. The transmission in the metallic state of the film is 𝒯ₒ. The horizontal x-axes of all the PT Is are normalized to 1. The equilibrium pressures used for the Van 't Hoff plots in Figure 2 are evaluated at x = 0.5. The harmonic mean temperature is T_{hm} = 404.8 K.

The PTIs for 67 different Mg_yTi_{1-y} alloys with 0.62 < y < 0.81 at 348, 383, 438 and 473 K obtained by means of hydrogenography (upon 1st hydrogenation) are shown in Figure 1. For Mg-rich alloys there are clear plateaus indicating the formation of transparent MgH_2 dihydrides. The isotherms get gradually more sloping when *y* approaches 0.62. This is due to an increasing admixture of Ti in the Mg-rich domains [42]. For each composition *y* the transmission $\ln(\mathcal{T}/\mathcal{T}_o)$ is normalized to its maximum value $[\ln(\mathcal{T}/\mathcal{T}_o)]_{max}$ and all the equilibrium pressures used to generate Van 't Hoff plots are taken at $[\ln(\mathcal{T}/\mathcal{T}_o)]/ [\ln(\mathcal{T}/\mathcal{T}_o)]_{max} = 0.5$. The enthalpy ΔH_i and entropy ΔS_i obtained from a linear fit to the individual Van 't Hoff plots are shown in Figure 2a. Both ΔH and ΔS increase as a function of the Mg/Ti fraction *y.* A linear relation between ΔH and ΔS is observed for 0.62 < y < 0.81 (Figure 2b). Note, that above y ~ 0.81 MgH_2 crystallizes in the rutile instead of the fcc phase, leading to a deviation from linearity.

The slope of the linear regression line defines the so-called compensation temperature

$$T_{comp} = \frac{d\Delta H}{d\Delta S} \tag{3}$$

We obtain T_{comp} = 470.1 ±1.3 K for the data in Figure 2b. While T_{comp} differs from the harmonic average temperature T_{hm} = 404.8 K, it still falls within the experimental range [348, 473 K] of temperatures. While this suggest a statistical origin of the ΔH -ΔS compensation, the large number of investigated samples (*N*=67) leads to a small standard error σ = 1.3 K for T_{comp}. The Krug-Hunter-Grieger criterion for an *EEC* of statistical origin[26]

$$T_{comp} - t\left[N = 67;\ 95\%\right]\sigma < T_{hm} < T_{comp} + t\left[N = 67;\ 95\%\right]\sigma \tag{4}$$

is clearly not satisfied as $t\left[N = 67; 95\%\right] \cong 2$. Accordingly, a non-statistical origin of the ΔH -ΔS compensation in Figure 2 is thus highly probable (at a 95% confidence level).

The very high value of the coefficient of determination R_{square} = 0.9995 of the experimental data in Figure 2 suggests that there should be a well-defined crossing of the 67 Van 't Hoff plots at T_{comp} = 470.10 K. Indeed, at the level of the P*T* Is in Figure 1 there is a clear indication that a genuine crossing of Van 't Hoff plots does exist: at temperatures 348, 383 and 438 K the equilibrium pressure for Mg_yTi_{1-y} alloys increases with increasing Mg concentration while at 473 K there is an opposite trend. This implies that somewhere in the interval between 438 and 473 K the equilibrium pressures should be essentially independent of the alloy composition, or, equivalently, that the spread of Van 't Hoff plots should have a minimum at a temperature T_{min} such that 438 < T_{min} < 473 K. This is immediately visible in Figure 2c, which shows the Van 't Hoff plots obtained from the enthalpy and entropy values in Figure 2a by means of

$$\ln P_i(T) = \frac{\Delta H_i}{R}\frac{1}{T} - \frac{\Delta S_i}{R} = h_i\frac{1}{T} - s_i \tag{5}$$

with $h_i = \Delta H_i / R$ and $s_i = \Delta S_i / R$. The index *i* runs from 1 to 67 and labels the Mg-Ti alloy compositions. For clarity at each temperature the average < ln*P* > taken over all y is subtracted from the $\ln P_i$.

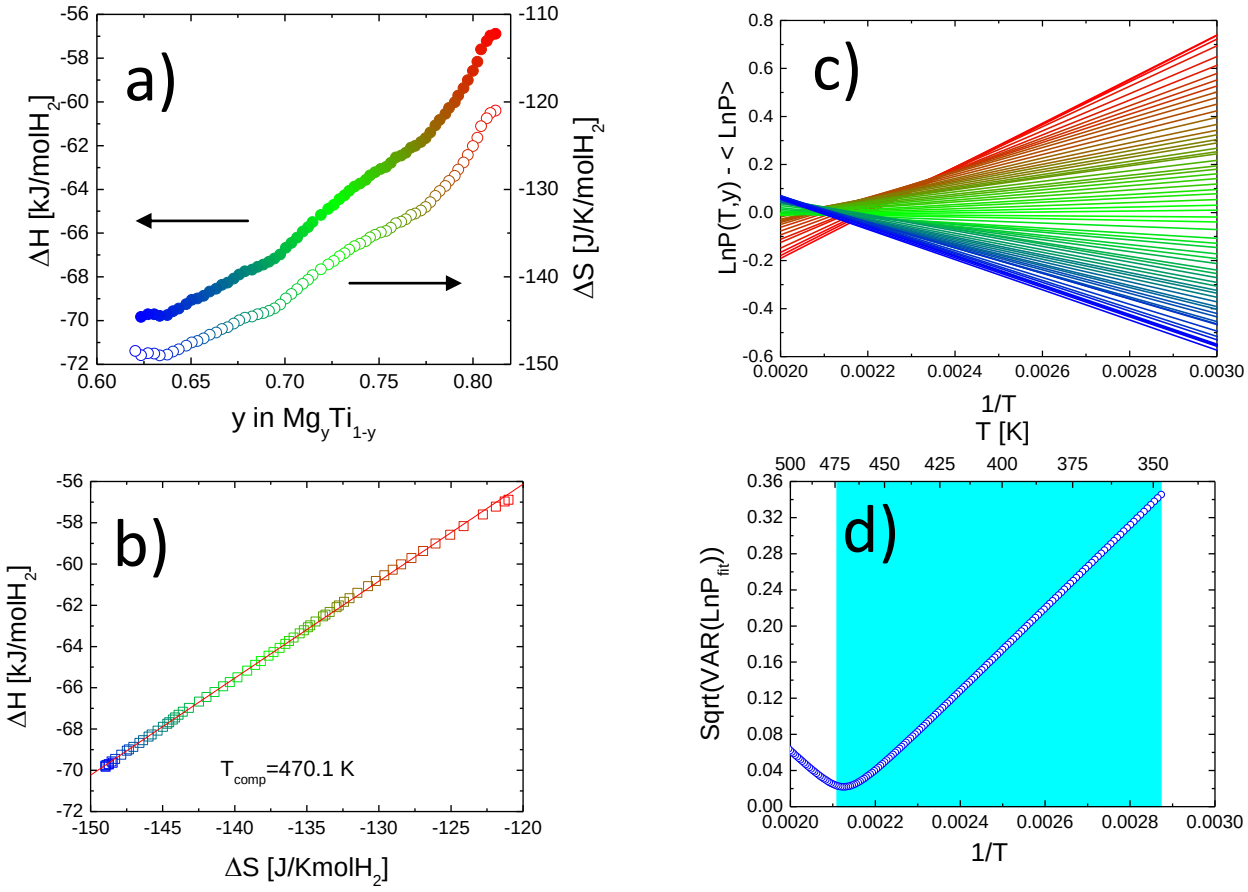

Figure 2: (a): Enthalpy (filled symbols) and entropy (open circles) for the 67 Mg_yTi_{1-y} alloys shown in Figure 1. (b): Enthalpy versus Entropy plot from the ΔH and ΔS values of the left panel. The compensation temperature is T_{comp} = 470.1 ± 1.3 K. The coefficient of determination of the fit is R_{square} = 0.9995 and T_{hm} = 404.8 K. The colours of the data points are the same as in Figure 1. (c): Van 't Hoff plots constructed from the ΔH and ΔS values in Figure 2a. For clarity at each temperature the average < ln$P$ > taken over all y is subtracted from the lnP_i . The colours of the data points are the same as in Figure 1. (d): Temperature dependence of the spread of lnP_i values calculated by means of Eq.6. The minimum spread occurs at T_{min} = 470.3 K. The experimental temperature range 348 to 473 K is indicated as blue rectangle.

To quantify the coalescence of the Van 't Hoff plots we define Ln*P*-Spread(*T*), the temperature dependent spread of Van 't Hoff plots, as follows

$$\text{Ln}P\text{-Spread}\,(T) = \sqrt{VAR\left(\ln P(T)\right)} \equiv \sqrt{\frac{1}{N-1}\sum_{i=1}^{N}\left(\ln P_i(T) - <\ln P(T)>\right)^2} \tag{6}$$

where *N* is the number of measured samples and the < > bracket indicates the average taken over all samples. Although Ln*P*-Spread(*T*) can directly be evaluated numerically from the Van 't Hoff plots (see fig. 2d), we derive in Section 2.3 of the Supplementary Information the following analytic expression

$$VAR\left(\ln P(T)\right) = \left(\left(\frac{1}{T}\right)^2 \times VAR(h) - \left(\frac{1}{T}\right)\frac{2N}{N-1}COVAR(h,s) + VAR(s)\right) \tag{7}$$

which shows explicitly that Ln*P*-Spread(*T*) is solely determined by the enthalpy and entropy variances and their enthalpy-entropy covariance

$$VAR(h) \equiv \frac{1}{N-1}\sum_{i=1}^{N}\left(h_i - <h>\right)^2 \tag{8}$$

$$VAR(s) \equiv \frac{1}{N-1}\sum_{i=1}^{N}\left(s_i - <s>\right)^2 \tag{9}$$

and

$$COVAR(h,s) = \frac{1}{N}\sum_{i=1}^{N}\left(h_i - <h>\right)\left(s_i - <s>\right) \tag{10}$$

From Eq.7 follows immediately that the smallest ln*P* spread occurs at the temperature

$$T_{\min} = \frac{(N-1)VAR(h)}{N \times COVAR(h,s)} \tag{11}$$

and is given by

$$\sqrt{VAR_{\min}} = \sqrt{VAR\left(\ln P\left(T_{\min}\right)\right)} = \sqrt{VAR(s) - \left(\frac{N}{N-1}\right)^2 \frac{\left(COVAR(h,s)\right)^2}{VAR(h)}} \tag{12}$$

The experimental data in Figure 2 lead to $VAR(\Delta H)$ = 14.70×10^6 J/(moleH_2) , $VAR(\Delta S)$ = 66.496 J/(K.moleH_2) and $COVAR\,(\Delta H, \Delta S)$ = 30.793×10^3 (J/moleH_2)^2/K and consequently to $VAR(h)$ = 212700 K^2 , $VAR(s)$ = 0.9620 and $COVAR(h,s)$ = 445.483 K. With these values we obtain $T_{\min}$ = 470.33 K and $\sqrt{VAR_{\min}} = 0.022$ in excellent agreement with the minimum in the calculated

curve based on Eq. 6 shown in Figure 2d. As a result of the very high value of the coefficient of determination R_{square} = 0.9995 of the ΔH versus ΔS fit, the difference between T_{comp} = 470.1 K and $T_{\min}$ = 470.33 K is very small. One has to realize, however, that these two temperatures are essentially different as T_{comp} is given by (see Section 2.2 of the Supplementary Information)

$$T_{comp} = \frac{N \times COVAR(h,s)}{(N-1) \times VAR(s)} \tag{13}$$

an expression that is clearly different from that in Eq.(11). This is explicitly shown in the next Section using the thermodynamic data derived from pressure composition isotherms measured by Syrenova et al[33] on Palladium nanocubes of various sizes.

2.2 Enthalpy-entropy compensation in Pd-H nanocubes

From the enthalpy and entropy values for the hydrogenation of Pd nanocubes[33] of sizes between 17 and 63 nm measured between 303 and 333 K , we obtain a linear ΔH and ΔS plot with R_{square}= 0.9793 (see Figure 3). The compensation temperature T_{comp} = 282.7 K is slightly lower than the lowest experimental temperature, 303 K. Classically, together with the relatively high value of the coefficient of determination R_{square}, this is an indication for a non-statistical behaviour. In addition, the Krug-Hunter-Grieger criterion[26] for a genuine, non-statistical *EEC* is met, since T_{hm} = 317.6 K falls just outside the statistical range [T_{comp}-2.2σ , T_{comp}+2.2σ]= [255, 310 K]. However, the large scatter in ΔH and ΔS data lead Syrenova et al. to conclude that the compensation effect is probably due to statistical effects[33]. Hence, according to the present understanding, it is difficult to decide whether a further analysis of a physical reason for the compensation effect is called for.

A much clearer picture emerges from our analysis shown in Figure 3c, obtained by generating Van 't Hoff plots from the enthalpy and entropy values in Figure 3a. We find that there is no well-defined crossing region. The Ln*P*-Spread(*T*) varies by only 25% within the experimental range 303-333 K. Quantitatively, our analysis of the Pd nanocube data yields $VAR(\Delta H)$ = 4.601×10^6 J/(moleH_2) , $VAR(\Delta S)$ = 56.389 J/(K.moleH_2) and $COVAR$ (ΔH, ΔS) = 14.713×10^3 (J/moleH_2)^2/K. The corresponding values $VAR(h)$ = 66559 K^2 , $VAR(s)$ = 0.8158 and $COVAR(h,s)$ = 212.85 K lead to $T_{\min}$ = 288.65 K and $\sqrt{VAR_{\min}} = 0.130$ in excellent agreement with the calculated curve in Figure 3d.

In the next two Sections we show that both the Mg-Ti alloy and the Pd-nanocube data lead naturally to the definition of a single parameter that

i) describes quantitatively the degree of coalescence of Van 't Hoff plots near $T_{\min}$ (or T_{comp}) without generating the Van 't Hoff plots from the ΔH and ΔS data)), and

ii) allows to characterize the likeliness of the statistical origin of the *EEC.*

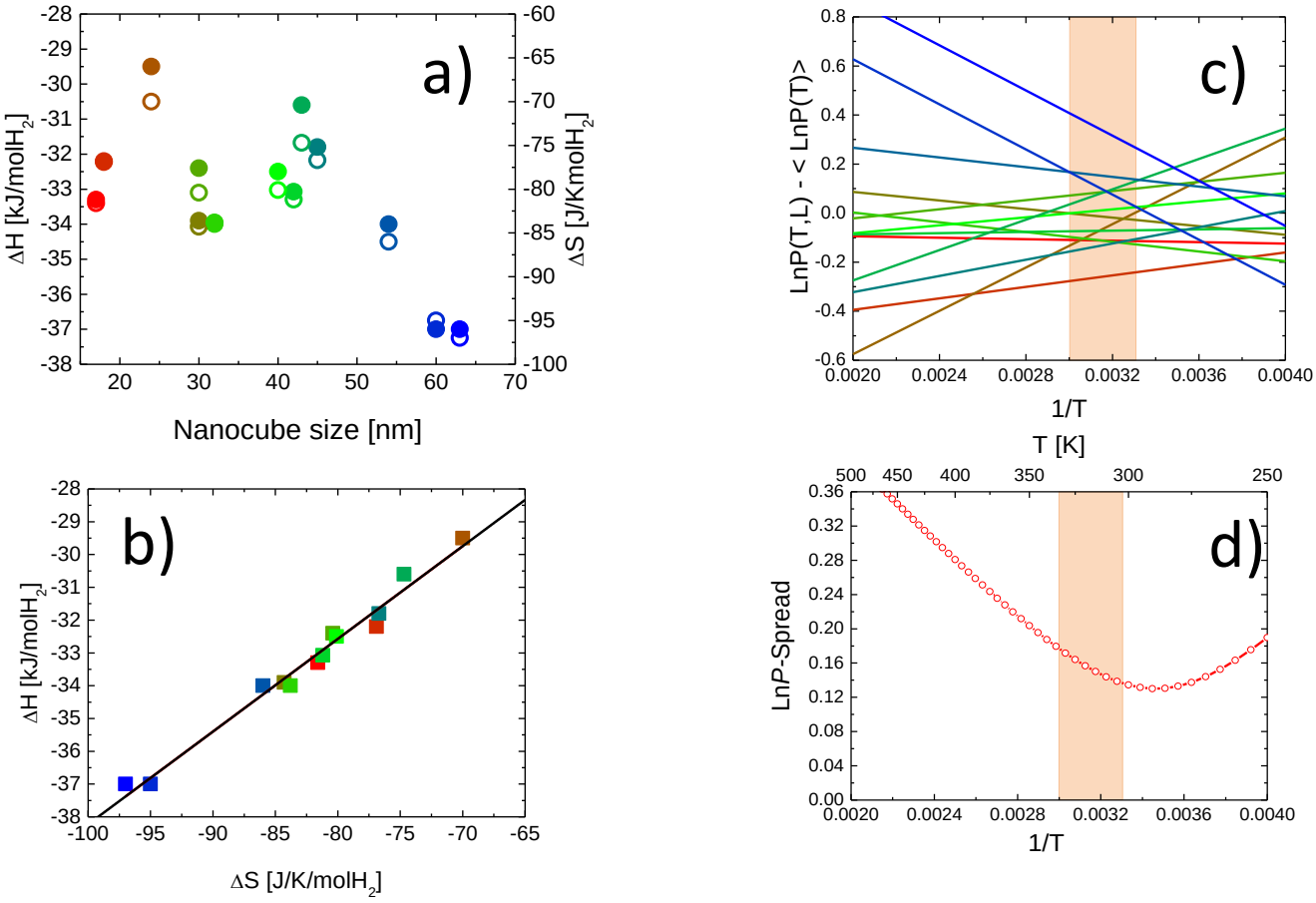

Figure 3: (a): Enthalpy (filled symbols) and entropy (open circles) for Pd nanocubes of sizes between 17 and 63 nm determined from pressure-composition isotherms between 303 and 333 K in Ref.33. (b): Corresponding ΔH versus ΔS plot. The compensation temperature is T_{comp}= 282.7 ± 12.4 K and lies, therefore outside the temperature range (303 – 333 K) of the measurements with average temperature T_{hm} = 317.6 K. The R_{square} is 0.97926;(c): Van 't Hoff plots constructed from the ΔH and ΔS values in Figure 3a. For clarity at each temperature the average < ln$P$ > taken over all nanocube sizes is subtracted from the individual ln$P$. The colours of the data points and lines in panels (a), (b) and (c) indicate the nanocube sizes; (d): Temperature dependence of the LnP-Spread calculated by means of Eq.(6). The minimum spread occurs at T_{min} =288.6 K. This value is in excellent agreement with the result predicted by the analytic Eq.(11). The experimental temperature range 303 to 333 K is indicated as coloured rectangle.

2.3 Compensation Quality Factor for the isoequilibrium region.

Although the R_{square} values for the thin film Mg_yTi_{1-y} alloys (R_{square} = 0.9995) and the Pd nanocubes (R_{square} = 0.97926) are both close to unity it is evident from Figure 2d and Figure 3d that the crossing region of the Van 't Hoff plots is much better defined for the Mg_yTi_{1-y} alloys. For the Mg_yTi_{1-y} alloys the Ln*P*-Spread varies by more than one order of magnitude within the experimental temperature range. For Pd nanocubes this spread varies only by 25%. This means that the minimum spread is only slightly smaller than the largest Ln*P*-Spread actually measured for the nanocubes. To quantify the essential difference between the Mg_yTi_{1-y} alloy and Pd nanocube data we introduce a Compensation Quality Factor (*CQF*) defined as

$$CQF = 1 - \sqrt{\frac{VAR_{\min}}{VAR_{\max}}} \tag{14}$$

where

$$VAR_{\min} \equiv VAR\left(\ln P\left(T_{\min}\right)\right) \tag{15}$$

is the minimum of the ln*P* variance and

$$VAR_{\max} \equiv VAR\left(\ln P\left(T*\right)\right) \tag{16}$$

is the largest variance of ln*P* actually measured in the experiment. As the variance is a quadratic function of (1/*T*) the largest variance occurs either at $T^* = T_{low}$ if 1/ $T_{\min}$ is closer to 1/ T_{high} or at $T^* = T_{high}$ if 1/ $T_{\min}$ is closer to 1/ T_{low}. The *CQF* is equal to 1 for a perfect compensation with all Van 't Hoff plots intersecting at a common isoequilibrium point in the pressure-temperature plane. In an experimental situation we always have to deal with experimental errors. The isoequilibrium point is then replaced by an isoequilibrium region characterized by a finite spread in ln*P* at $T_{\min}$. Speaking of an isoequilibrium region is only meaningful if the Ln*P*-Spread at $T_{\min}$ is clearly smaller than the largest spread observed in the experiment. Hence, we choose as isoequilibrium criterion

$$CQF > 0.9 \tag{17}$$

which means that Ln*P*-Spread at $T_{\min}$ needs to be 10 times smaller than at the temperature *T**. As from Eq.(7)

$$VAR_{\max} = \left(\left(\frac{1}{T*}\right)^2 VAR(h) - \frac{1}{T*}\frac{2N}{N-1}COVAR\left(h,s\right) + VAR(s)\right) \tag{18}$$

we find then with *T**(MgTi*)* = 348 K and *T** (Pd*)*=333 K, $\sqrt{VAR_{\max}\left(\text{Mg-Ti alloys}\right)} = 0.345$ and $\sqrt{VAR_{\max}\left(\text{Pd nanocubes}\right)} = 0.176$. From Eq.(14) and the minimum variances indicated above we obtain

CQF (67 Mg-Ti alloys) = 0.937 (19)

and

CQF (13 Pd nanocubes) = 0.262 (20)

This means that the isoequilibrium criterion Eq.(17) for a well-defined crossing region of Van 't Hoff plots is only satisfied for the Mg-Ti alloys and not at all for the Pd-nanocubes. The definition of CQF in Eq.(14) is solely based on the measured Van 't Hoff plots and does not depend on whether $T_{\min}$ falls within or outside the range of measurements.

In literature many articles do not show the Van 't Hoff plots but list the derived enthalpies and entropies. It is therefore useful to express the CQF directly in terms of ΔH-ΔS data. This is readily obtained by noting that the coefficient of determination R_{square} of a ΔH versus ΔS plot (such as those in Figure 2 and Figure 3) is given by Eq.S21 in the Supplementary Information,

$$R_{square} = \frac{N^2}{(N-1)^2} \frac{\left(COVAR(h,s)\right)^2}{VAR(s) \times VAR(h)} \tag{21}$$

From Eqs.(11), (13) and (21) follows then

$$CQF = 1 - \sqrt{\frac{1-R_{square}}{\left(\frac{1}{R_{square}}\right)\left(\frac{T_{comp}}{T^*}\right)^2 - 2\frac{T_{comp}}{T^*} + 1}} \tag{22}$$

Equation (22) is especially interesting as it expresses CQF in terms of the parameters R_{square} and T_{comp} that are directly obtained from a linear fit to enthalpy and entropy data for a given set of experiments. It is well suited to understand how the Compensation Quality Factor depends on the quality of the linear fit of the ΔH versus ΔS plot, which is usually taken as the value of the R_{square} parameter. Equation (22) shows explicitly that values of R_{square} very close to 1 are needed to satisfy the isoequilibrium criterion in Eq.(17). This key result is easily illustrated by using in (22) the same characteristic temperatures T_{comp} = 432.9 K and T^* = 348 K as for the Mg-Ti alloys. In order to satisfy the criterion in Eq. (17) we need R_{square} > 0.99875. Similarly for the nanocubes with T_{comp} = 432.9 K and T^* = 333 K, R_{square} > 0.99977 is needed. In other words R_{square} is not an adequate indicator of a well-defined isoequilibrium point. Linear ΔH versus ΔS plots are easily obtained even for sets of Van 't Hoff plots with a low CQF. This is demonstrated in Section 4 of the Supplementary information where we show that an extremely high R_{square} = 0.99987 can still lead to a rather low CQF if the average experimental temperature is close to T_{comp} and the denominator in Eq.(22) is small.

2.4 CQF parameter as discriminator for a non-statistical origin of Enthalpy-Entropy Compensation

As described in the introduction a fundamental question about *EEC* is whether or not the linear relation is due to statistical errors or due to a genuine physical/chemical/biological compensation. We show here that the *CQF* can indeed provide a way to answer this question quantitatively. Specifically we show that it is extremely unlikely that data satisfying the criterion *CQF* > 0.9 are the result of independent statistical errors.

For this we ran a large number of simulations in which we randomly generated Van 't Hoff plots for *N* = 4, 8, 16 and 32 samples in the temperature interval [T_{low}, T_{high}]. The only constraint is that the random pressures are drawn independently within a chosen interval [lnP_{min}(T_{low}), lnP_{max}(T_{low})] and [lnP_{min}(T_{high}), lnP_{max}(T_{high})]. More details about the simulations are given in Section 3 of the Supplementary Information. For each simulation we calculate T_{comp}, R_{square}, T_{min} and *CQF* . The distribution of simulated *CQF* values are shown as histograms in Figure 4.

For *N* = 4 the values of *CQF* are spread between 0 and almost 1, whereas with increasing number of samples the *CQF* distribution is compressed towards increasingly lower values. Clearly, *CQF* values close to one become less likely with increasing number of samples *N*, as shown by the cumulative percentage curves in blue. Defining a threshold value $\gamma[N;\ \mathrm{CL\%}]$ as a function of the number of samples *N* and the confidence level CL%, we observe that 99% of the simulated *CQF* values are smaller than γ = 0.935, γ = 0.728, γ = 0.586 and γ = 0.487 for *N* = 4, 8, 16 and 32 samples, respectively. These threshold values depend of course on the choice of the confidence level CL% and are well described by

$$\gamma\left[N;\ 95\%\right] = 0.29 + 1.43 / N^{0.67} \tag{23}$$

$$\gamma\left[N;\ 99\%\right] = 0.29 + 1.41 / N^{0.57} \tag{24}$$

$$\gamma\left[N;\ 99.5\%\right] = 0.29 + 1.39 / N^{0.53} \tag{25}$$

These lines are plotted in the middle panel of figure 4: If the *CQF* falls within the red-dotted region the simulations indicate that the *EEC* is of statistical origin at a 99% confidence level. The asymptotic value $\gamma[N \to \infty;\ \mathrm{CL\%}] = 1 - 1/\sqrt{2} \cong 0.29$ is given in Eq.S49.

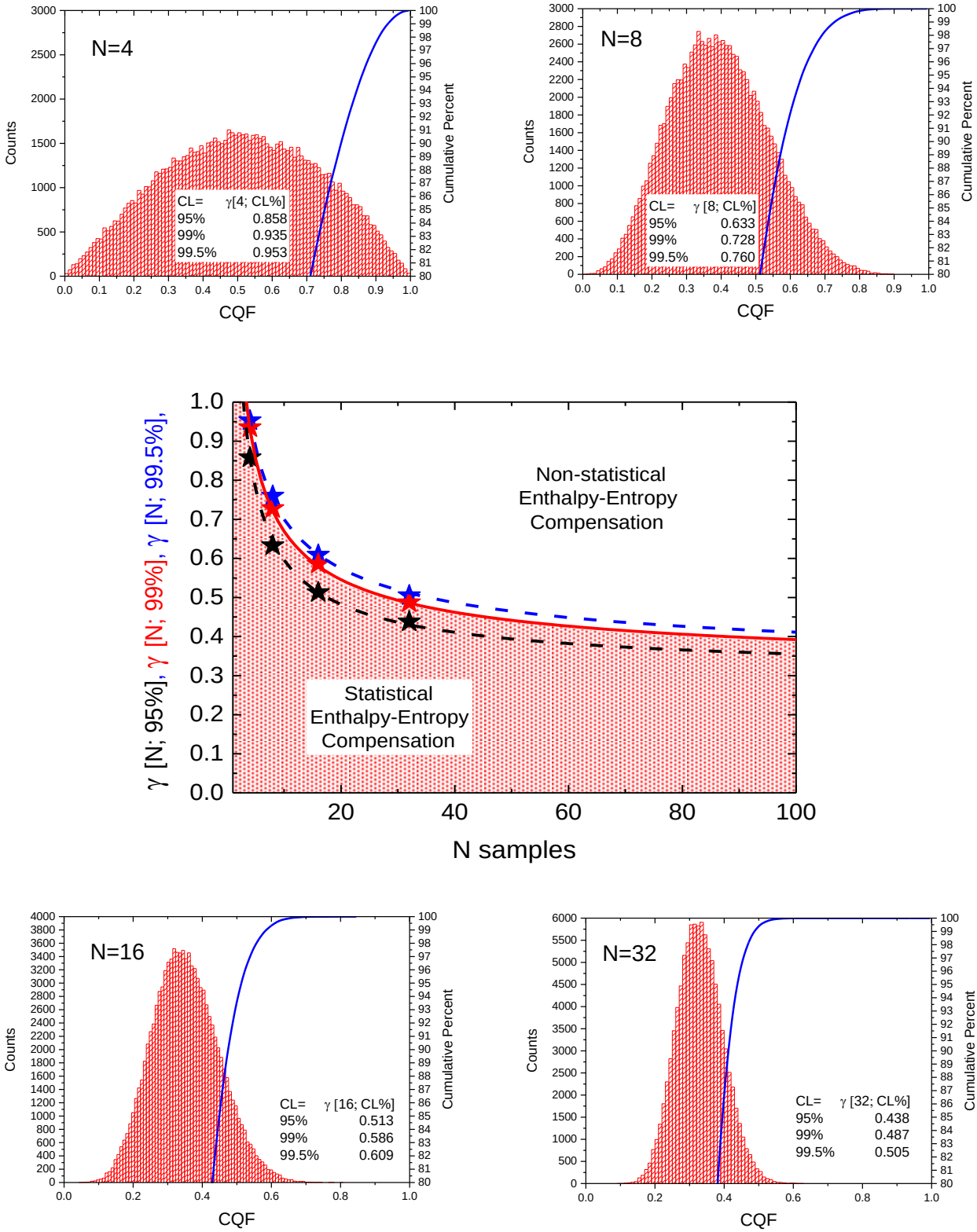

Figure 4: Histograms and cumulative percents for the *CQF* parameter obtained from 10^5 simulations with randomly generated van 't Hoff plots for *N* = 4, 8, 16 and 32 samples. Details of the simulations are given in Section 3 of the Supplementary Information. The threshold *CQF* values γ [*N*; CL%] for 95% (black dashed line), 99% (red line) and 99.5% (dashed blue line) confidence levels indicated in the central panel are well described by the simple algebraic relations given in Eqs. (23), (24) and (25), respectively. If the *CQF* falls within the red-dotted region the simulations indicate that the *EEC* is of statistical origin at a 99% confidence level.

For a 99% confidence level Eq.(24) implies that $\gamma[N{=}5;\ 99\%] \cong 0.853$ and there is only a 1% chance that a *CQF* larger than this value is due to statistical effects. As $\gamma[N;\ 99\%]$ is a decreasing function of *N* the following three cases may occur when $N \geq 5$:

a) When $CQF \geq 0.9 > \gamma[N;\ 99\%]$ the isoequilibrium criterion is satisfied and the Van 't Hoff plots coalesce in a small region of the pressure-temperature plane. There is a 99% chance that the *EEC* is of non-statistical (i.e. physical, chemical or biological) origin.

b) When $0.9 > CQF \geq \gamma[N;\ 99\%]$ the *EEC* is of non-statistical (i.e. physical, chemical or biological) origin. The crossing of the Van 't Hoff lines occurs over a wider region of the *p*-*T* plane.

c) When $\gamma[N;\ 99\%] > CQF$ the *EEC* is of statistical origin and there is essentially no coalescence of Van 't Hoff lines. For example, for *N* = 10 samples, $\gamma[N;\ 99\%] = 0.67$. A *CQF* smaller than 0.67 implies that Ln*P*-Spread at T_{min} is only 3 times smaller than the largest measured Ln*P*-Spread.

We have now all the ingredients to draw conclusions about the Mg-Ti alloys and Pd-nanocube data for which

$$CQF(67\ \text{Mg-Ti alloys}) = 0.937 > 0.418 = \gamma\left[N = 67;\ 99\%\right] \tag{26}$$

and

$$CQF(13\ \text{Pd nanocubes}) = 0.262 < 0.617 = \gamma\left[N = 13;\ 99\%\right] \tag{27}$$

The large *CQF* value for the 67 Mg-Ti alloys, which satisfies the isoequilibrium criterion Eq.(17), is much higher than the threshold $\gamma[N{=}67;\ 99\%]$ and a statistical origin of the observed *ΔH-ΔS* compensation in Figure 2b can safely be discarded. For Pd-nanocubes, however, the linear *ΔH versus ΔS* plot is probably due to statistical errors since *CQF* is much smaller than $\gamma[N{=}13;\ 99\%]$. This conclusion is confirmed by the analysis of hydrogenation data of Pd nanocubes reported by various research groups in ref.40.

The method described so far can easily be used to analyze any (published) *ΔH-ΔS* data. In the Supplementary Information we apply it to the largest *ΔH-ΔS* data set ever published. The latter data[20] are obtained for hydrogen absorption obtained in parallel from 3859 $Mg_yNi_zTi_{1-y-z}$ thin film alloys and provide an additional insight about *ΔH-ΔS* compensation and correlation as well as isoequilibrium temperature in systems with very large numbers of samples. For example, 668 $Mg_yNi_zTi_{1-y-z}$ samples with a high Mg-content ($0.79 < y < 0.86$) have a *ΔH-ΔS* compensation with $R_{square} = 0.99833$ and $T_{comp} = 379.4$ K. The Compensation Quality Factor is *CQF* = 0.812 and all the Van 't Hoff plots cross in a relatively small region of the pressure-temperature plane. Although the *CQF* does not fully satisfy our isoequilibrium criterion it is very important to realize that for *N* = 668, $\gamma[N{=}668;\ 99\%] = 0.325$ and $\gamma[N{=}668;\ 99.5\%] = 0.335$. The much larger value of *CQF* implies thus that the observed *EEC* is necessarily of physical origin. Another valuable insight that is provided by the large body of $Mg_yNi_zTi_{1-y-z}$ alloys data, relates to the non-linear *ΔH-ΔS* correlations that exist for families of samples. For example, for the 39 $Mg_yNi_zTi_{1-y-z}$ samples with Ni = 0.3 $\pm$ 0.002 the (*ΔH, ΔS*) points lie on half an elongated ellipse. There is therefore a high degree of

correlation but the coefficient of determination R_{square} = 0.84 and *CQF* = 0.29 are relatively small and there is no *EEC*.

2.5 Quality Factor for isokinetic relationship

The analysis developed in the previous sections can be applied straightforwardly to kinetic studies. The rate constant *k* of thermally activated processes is usually well described by an Arrhenius expression [43].

$$k = Ae^{-\frac{E^a}{RT}} \tag{28}$$

where E^a is the apparent activation energy. Equation(28) implies that a plot of ln k_i measured for sample versus the reciprocal temperature is a straight line with slope E_i^a/R and intercept lnA_i. With these fitted values one can generate lnk_i by means of

$$\ln k_i\left(T\right) = \ln A_i - \frac{E_i^a}{RT} \tag{29}$$

From a comparison of Eq.(29) with Eq.(2) we see the following correspondence between the enthalpy and entropy for *equilibrium* measurements and the activation energy and prefactor of *kinetic* measurements

$$\begin{aligned} \Delta H_i &\leftrightarrow -E_i^a \\ \Delta S_i &\leftrightarrow -R\times\ln A_i \end{aligned} \tag{30}$$

All the relations derived for the equilibrium measurements can therefore be adapted to the analysis of kinetic data by using the substitutions in Eq.(30). To illustrate this we analyze the kinetic data of the Mg-based hydrides reported by Andreasen et al.[28]. The values of activation energies and prefactors obtained from a linear fit to rate constants measured during dehydrogenation of 8 samples are shown in Figure 5.
The slope of this modified Cremer-Constable plot [43], the so-called isokinetic temperature T_{isokin}

$$T_{isokin} = \frac{dE^a}{R\times d\ln A} \tag{31}$$

is the analog of the compensation temperature T_{comp} introduced in Eq.(3).
The Compensation Quality Factor for kinetic data is given by the same expression as Eq.(22) with T_{comp} replaced by T_{isokin}

$$CQF = 1-\sqrt{\frac{1-R_{square}}{\left(\frac{1}{R_{square}}\right)\left(\frac{T_{isokin}}{T^*}\right)^2 - 2\frac{T_{isokin}}{T^*}+1}} \tag{32}$$

with, as shown in Section 2.4 in the Supplementary Information,

$$R_{square} = \frac{N^2}{(N-1)^2} \frac{\left(COVAR\left(E^a, \ln A\right)\right)^2}{VAR\left(E^a\right) \times VAR(\ln A)} \tag{33}$$

$$T_{isokin} = \frac{1}{R}\left(\frac{N}{N-1}\right)\frac{COVAR(E^a, \ln A)}{VAR(\ln A)} \tag{34}$$

$$T_{\min} = \frac{1}{R}\left(\frac{N-1}{N}\right)\frac{VAR\left(E^a\right)}{COVAR\left(E^a, \ln A\right)} \tag{35}$$

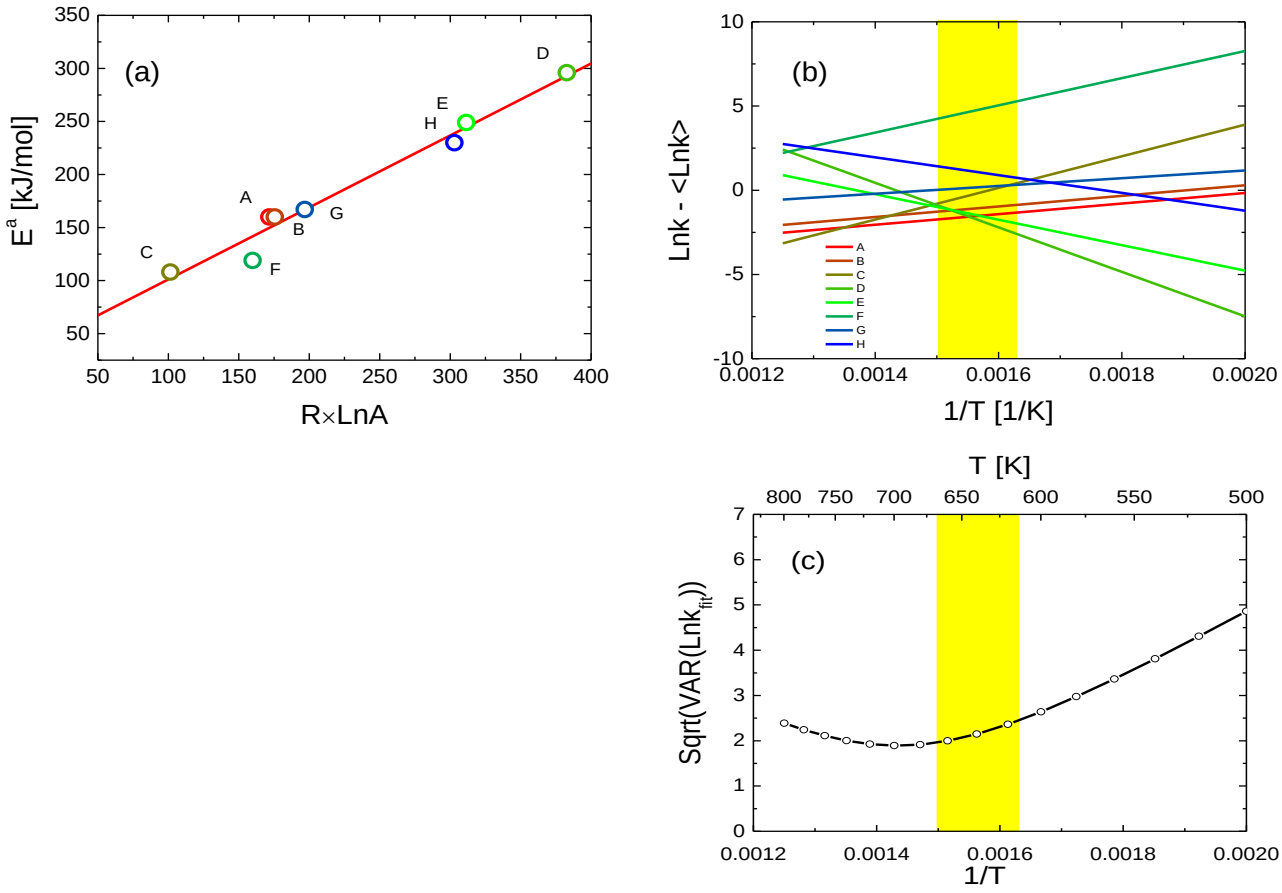

Figure 5: *a*) Modified Cremer - Constable plot of the kinetic dehydrogenation data of the 8 Mg based hydrides given in Table 1 of reference 28. The isokinetic temperature is T_{isokin}= 678.4 K and the coefficient of determination R_{square} is 0.973. *b*) Arrhenius plots constructed from the E^a and *R*ln*A* values in panel *a*). For clarity at each temperature the average < ln*k* > taken over the 8 hydrides is subtracted from the individual ln*k* . The colours of the lines are the same as in a). *c*) Temperature dependence of the spread of ln*k* values calculated by means of Eq.(29). The minimum spread occurs at T_{min} = 697.3 K. This value is in excellent agreement with the result predicted by the analytic Eq.(35). The experimental temperature range 629 to 662 K is indicated as yellow rectangle. Within this range the spread of ln*k* varies only little. This leads to the small *CQF* = 0.162.

For the dehydrogenation of the 8 Mg-based hydrides the experimental data in

Figure 5 Eq.(32) together with T^* = 629 K leads to

$$CQF = 0.162 \tag{36}$$

Although R_{square} = 0.973 is close to unity the low value of the *CQF* indicates that there is no well-defined isokinetic region. This is mainly due to the narrow range of experimental temperatures, 629 to 662 K, which is only 5% of the average temperature. Furthermore, as

$$CQF(8\ \text{Mg samples}) = 0.162 < 0.721 = \gamma\left[N = 8;\ 99\%\right] \tag{37}$$

we conclude within a 99% confidence level that the E^a versus ln*A* compensation is of statistical origin. In the Supplementary Information we apply it to the thermodynamic activation parameters of fish myofibrillar ATPase enzyme.[4444,4545]

3 Conclusions

The Compensation Quality Factor *CQF* plays a pivotal role in the characterization of an Enthalpy-Entropy Compensation (*EEC*). Before summarizing its main properties we provide a quick recipe for its determination. For this we assume that the enthalpy $h_i = \Delta H_i / R$ and entropy $s_i = \Delta S_i / R$ for a series of *N* samples (i=1,...,*N*) have been determined from measurements within the temperature range [T_{low}, T_{high}]. The existence of a genuine isoequilibrium state and the likeliness of a non-statistical origin of the *EEC* are then easily evaluated following the steps:

1. Using standard software (for example Excel) calculate the variances *VAR*(*s*), *VAR*(*h*) and covariance *COVAR*(*h,s*)
2. Calculate with Eq.11, $T_{\min}=(N-1)VAR(h)/N/COVAR(h,s)$
3. Calculate with Eq.12, $VAR_{\min}=VAR(s)-[N/(N-1)COVAR(h,s)]^2/VAR(h)$
4. Determine T^* from the condition: If $|1/T_{\min} - 1/T_{high}| < |1/T_{\min} - 1/T_{low}|$ then $T^*=T_{low}$ otherwise $T^*=T_{high}$
5. Calculate with Eq.18, $VAR_{\max}=(1/T^*)^2 VAR(h)-2N/(N-1)(1/T^*)COVAR(h,s)+VAR(s)$
6. The Compensation Quality Factor *CQF* is then simply $CQF=1-(VAR_{\min}/VAR_{\max})^{1/2}$

The power of the single *CQF* value is to characterize quantitatively both the degree of coalescence of Van 't Hoff plots and the probability of the statistical origin of the Enthalpy-Entropy Compensation (*EEC*):

A. A genuine isoequilibrium state exists if *CQF* > 0.9. This condition guarantees that the minimum spread in the *N* Van 't Hoff plots is one order of magnitude smaller than the largest measured spread.

B. At a 99% confidence level the observed *EEC* is a real effect, i.e. not due to a statistical artefact if $CQF > \gamma[N;99\%] = 0.29+1.41/N^{0.57}$

With this procedure we have established that for the 67 thin Mg-Ti –H films, *CQF* = 0.937 while *CQF* = 0.262 for the 13 Pd-H nanocubes. We conclude therefore that a true coalescence of Van 't Hoff plots occurs only for the Mg-Ti alloys.

Furthermore, from $CQF(67\ \text{Mg-Ti alloys}) = 0.937 > \gamma\left[N = 67;\ 99\%\right]$ and $CQF(13\ \text{Pd nanocubes}) = 0.262 < \gamma\left[N = 13;\ 99\%\right]$ it follows that at a 99% confidence level the *EEC* for the Mg-Ti-H films is a genuine compensation effect, while it is of statistical origin for the Pd-H nanocubes.

Although experimental data for metal-hydrides have been used in this work, *any* results obtained from equilibrium measurements based on Van 't Hoff plots as well as from kinetic measurements based on Arrhenius plots can be analyzed with the method described in this work. This is explicitly demonstrated for the dehydrogenation kinetics of 8 Mg-based hydrides and the thermodynamic activation parameters of fish myofibrillar ATPase enzyme. The CQF values $CQF(8\ \text{Mg samples}) = 0.162$ and $CQF(7\ \text{Fishes}) = 0.746$ are too low for a clear isokinetic state. As γ[*N*=8; 99%] ≅ 0.72 the *EEC* observed for the 8 Mg samples is of statistical origin. For the 7 fishes the situation is borderline as γ[*N*=7; 99%] ≅ 0.755 is very close to the *CQF* value.

An attractive feature of our analysis is that *CQF* depends only on enthalpy and entropy values and the experimental temperature range. This is a great advantage for the evaluation of published data for which very often Van 't Hoff data are not available.

Finally, it is important to mention that the very large data set for hydrogen absorption in 3859 $Mg_yNi_zTi_{1-y-z}$ alloys exhibit a high degree of enthalpy-entropy correlation that is not always linear. However, for some large families of alloys (for example the 668 Mg rich alloys) *EEC* does occur with *CQF* much larger than γ[*N*=668; 99%] implying a non-statistical origin of the *EEC.*

4 Experimental Section

4.1 Mg-Ti sample preparation

Mg_yTi_{1-y} thin films with a compositional gradient are prepared in a 7-gun ultra-high-vacuum dc/rf magnetron co-sputtering system (AJA Int., base pressure 10^{-7} Pa) at room temperature and in 3 µbar of Ar on 50x5 mm^2 quartz substrates. Mg and Ti are facing each other in tilted off-axis sputtering guns. By adjusting the power applied to each gun the desired region of the binary phase diagram is obtained. The Mg fraction of the 50 nm Mg_yTi_{1-y} films along the length of the sample varies between $0.62 \leq y \leq 0.81$. The Mg films is sandwiched between two 10 nm Fe layers and capped by 10 nm Pd. The iron layers serve to minimize the interaction of the Mg with the substrate and the Pd layer. The latter promotes H_2 dissociation and prevents oxidation of the underlying film. While the Fe and Pd are deposited on a rotating substrate resulting in uniform thicknesses, the Mg_yTi_{1-y} compositional gradient layer is obtained by co-sputtering from Mg and Ti sources tilted towards a stationary substrate. The composition of the films is gauged by measuring the thickness gradients of single element films. The same sputtering system is used for ternary $Mg_yNi_zTi_{1-y-z}$ gradient thin films described in the Supplementary information. In this case, the Mg, Ti and Ni off-axis sputter guns are positioned every 120° on a circle and 3-inch diameter sapphire substrates are used.[20]

4.2 Hydrogenography

After deposition, metallic films are transferred into an optical cell to monitor their optical transmission during hydrogenation.[20] The whole cell is placed in an oven to control temperature up to 300°C. The complete thermal equilibration of the setup is checked by comparing the output of two PT100 resistors placed at different locations in the oven, one of them being in contact with the sample holder. A 150 W diffuse white light source illuminates the sample from the substrate side, and a 3-channel (RGB) SONY XC-003 charged-coupled device (CCD) camera continuously monitors the transmitted light as a function of hydrogen pressure. The 3-channel transmission intensities are added, resulting in a 1.1 to 3.3 eV photon energy bandwidth. The transmission intensity is integrated over the width of the sample as no significant change of composition or thickness occurs across this direction. The gas pressure increase is controlled by a MKS 248/250 forward Proportional-Integral-Differential (PID) system that regulates both inlet and outlet gas flows. 0.1% to 100% hydrogen in argon mixtures are used to achieve hydrogen (partial) pressures of between $10^{-1} < p(H_2) < 10^6$ Pa. Typical pressure sweeps have a duration of 8.6×10^4 s.
The Pressure-Transmission-Isotherms (PT Is) for the Mg-Ti samples are obtained by measuring the optical transmission of every spot (expressed in pixels) of the gradient sample as recorded by the 3CCD camera. The transmission data are averaged in a direction perpendicular to the composition gradient. The background pressure of the cell is 10^{-2} Pa. The hydrogen pressure is gradually increased exponentially from 4 to 300 kPa, depending on the temperature. For this purpose, a 4% H_2/Ar gas mixture and pure (100%) H_2 gas are used with a gas flow set to 20 sccm. Thus, in the gradient Mg_yTi_{1-y} thin films the hydrogenation is optically monitored for all compositions *simultaneously*, which minimizes systematic experimental errors, the hydrogen gas pressure and the temperature being exactly the same for all samples. More details about Hydrogenography of 3859 Mg-Ti-Ni samples are given in refs. [46] and [47].

AUTHOR INFORMATION

Corresponding Authors:
*E-mail: b.dam@tudelft.nl and r.p.griessen@vu.nl

Note: The authors declare no competing financial interest.

KEYWORDS: Compensation, hydrides, Kinetics, Statistics, Thermodynamics

ACKNOWLEDGEMENTS

This work is part of the research of the Stichting voor Fundamenteel Onderzoek der Materie (FOM), which is financially supported by the Nederlandse Organisatie voor Wetenschappelijk Onderzoek (NWO).

Author Contributions

C. Boelsma. and R. Griessen developed the Enthalpy-Entropy Compensation verification method. C. Boelsma, R. Gremaud. and Ch.P. Broedersz designed and performed the experiments and analyzed data. H. Schreuders prepared the samples and provided technical support. R. Griessen and B. Dam wrote and edited the manuscript and supervised the project.

REFERENCES

[1] E. Cremer, *Adv. Catal.* **1955,** *7*, 75-91.

[2] M. C. Wilson, A. K. Galwey, *Nature* **1973**, *243*, 402–404.

[3] D. McPhail, A. Cooper, *J. Chem. Soc., Faraday Trans.* **1997**, 93, 2283-2289.

[4] L. Liu, Q. X. Guo, *Chemical Reviews* **2001**, *101*, 673-696.

[5] T. Bligaard, K. Honkala, A. Logadottir, J. K. Nørskov, S. Dahl, C. J. H. Jacobsen, *The Journal of Physical Chemistry B,* **2003,** *107,* 9325–9331.

[6] D. Teschner, G. Novell-Leruth, R. Farra, A. Knop-Gericke, R. Schlögl, L. Szentmiklósi, N. López, *Nat. chem.* **2012,** *4*, 739-745.

[7] J. C. Gehrig, M. Penedo, M. Parschau, J. Schwenk, M. A. Marioni, E.W. Hudson, H.J. Hug, *Nat. commun.* **2017,** *8,* 1-8.

[8] D. Asnin, Leonid, Maria V. Stepanova, *J. Sep. sci.* **2018,** *41,* 1319-1337.

[9] R. Lumry, S. Rajender, *Biopolymers* **1970,** *9,* 1125–1227.

[10] B. Rosenberg, G. Kemery, R. C. Switcher, T. C. Hamilton, *Nature* **1971**, *232,* 471–473.

[11] J. Petruska, M. F. Goodman, *J. Biol. Chem.* **1995**, *270,* 746-750.

[12] L. Liu, C. Yang, Q. Guo, *Biophys. Chem.* **2000**, *84,* 239–251.

[13] A. I. Dragan, C.M. Read, C. Crane-Robinson, Eur. Biophys. J. **2017**, *46,* 301-308.

[14] T.S.G. Olsson, J. E. Ladbury, W. R. Pitt, M. A. Williams, *Protein Sci.* **2011**, *20,* 1607-1618.

[15] N. Tang, L.H. Skibsted, Food Res. Int. **2016**, *89,* 749-755.

[16] J. A. Schwarz, L. E. Felton, *Solid-State Electronics* **1985**, *28,* 669–675.

[17] U. Lubianiker, I. Balberg, *Phys. Rev. Lett.* **1997**, *78,* 2433–2436.

[18] R. Widenhorn, L. Mündermann, A. Rest, E. Bodegom, *J. Appl. Phys.* **2001**, *89,* 8179–8182.

[19] M. Ullah, T. B. Singh, H. Stifler, N. S. Sariciftci, *Appl. Phys. A* **2009**, *97,* 521–526.

[20] R. Gremaud, , Ch.P. Broedersz, D.M. Borsa, A. Borgschulte, P. Mauron, H. Schreuders, J.H. Rector, B. Dam, R. Griessen, *Adv. Mater.* **2007**, *19,* 2813-2817.

[21] O. Exner, *Nature* **1964**, *201,* 488–490.

[22] O. Exner, *Nature* **1970**, *227,* 366–367.

[23] B. E. C. Banks, V. Damjanovic, C. A. Vernon, *Nature* **1972**, *240,* 147–148.

[24] G. Kemeny, B. Rosenberg, *Nature* **1973**, *243,* 400–401.

[25] P. S. Harris, *Nature* **1973**, *243,* 401–402.

[26] R. R. Krug, W. G. Hunter, R. A. Grieger *Nature* **1976,** *261,* 566-567.

[27] A. Cornish-Bowden, *J. Biosci.* **2002**, *27,* 121–126.

[28] A. Andreasen, T. Vegge, A. S. Pedersen, *J. Phys. Chem. B.* **2005**, *109,* 3340–3344.

[29] P.J. Barrie, *Phys. Chem. Chem. Phys.* **2012**, *14,* 318-326.

[30] P. J. Barrie, *Phys. Chem. Chem. Phys.* **2012**, *14,* 327-336.

[31] R. R. Krug, W. G. Hunter, R. A. Grieger, *J. Phys. Chem.* **1976**, *80,* 2335-2341.

[32] R. R. Krug, W. G. Hunter, R. A. Grieger, *J. Phys. Chem.* **1976**, *80,* 2341–2351.

[33] S. Syrenova, C. Wadell , F. A. Nugroho, T. A. Gschneidtner, Y. A. Fernandez, G. Nalin, D. Świtlik , F. Westerlund, T. J. Antosiewicz, V. P. Zhdanov, K. Moth-Poulsen*, Nature Mater.* **2015**, *14,* 1236-1245.

[34] I. A. Johnston, G. Goldspink, *Nature* **1975,** *257,* 620-622.

[35] R. Bardhan, L. O. Hedges, C. L. Pint, A. Javey, S. Whitelam, J. J. Urban, *Nature Mater.* **2013,** *12,* 905–912.

[36] T. B. Flanagan, S. Luo, *J. Phase Equilib. Diffus.* **2007,** *28,* 49–57.

[37] M. Yamauchi, R. Ikeda, H. Kitagawa, M. Takata, *J. Phys. Chem. C* **2008**, *122,* 3294–3299.

[38] F. M. Mulder, S. Singh, S. Bolhuis, S. W. H. Eijt, *J. Phys. Chem. C* **2012**, *116,* 2001–2012.

[39] A. Anastasopol, T. V. Pfeiffer, J. Middelkoop, U. Lafont, R. J. Canales-Perez, A. Schmidt-Ott, F. M. Mulder, S. W. Eijt, *J. Am. Chem. Soc.* **2013**, *135,* 7891–7900.

[40] R. Griessen, N. Strohfeldt, H. Giessen, *Nature mater.* **2016**, *15,* 311-317.

[41] F.D. Manchester, Phase diagrams of binary hydrogen alloys. ASM International, Member/Customer Service Center, Materials Park, OH 44073-0002, USA. ISBN 0-87170-587-7 **2000**. 322.

[42] R. Gremaud, A. Baldi, M. Gonzalez-Silveira, B. Dam & R. Griessen, *Phys. Rev. B* **2008,** *77*, 144204.

[43] G. C. Bond, M.A. Keane, H. Kral, H., & J.A. Lercher, *Catalysis Reviews* **2000**, *42,* 323-383.

[44] A. Cornish-Bowden, *Journal of biosciences* **2017**, *42,* 665-670.

[45] I.A. Johnston & G. Goldspink, *Nature* **1975**, *257,* 620-622 (1975).

[46] R. Gremaud, Hydrogenography. A thin film optical combinatorial study of hydrogen storage materials. PhD thesis. VU University, Amsterdam. ISBN/EAN 978-90-9023439-7 (**2008**).

[47] Y. Pivak, Validation of hydrogenography for the search of promising hydrogen storage materials. PhD thesis. VU University Amsterdam & Delft University of Technology, Amsterdam & Delft. ISBN/EAN 978-94-6108-260- 2 (**2012**).